Fireball Interaction with Lithium Mist in Light Ion Beam Driven Fusion Reactor Cavities

R.R. Peterson

August 1983
(revised March 1984)

UWFDM-536

FUSION TECHNOLOGY INSTITUTE

UNIVERSITY OF WISCONSIN

MADISON WISCONSIN

Fireball Interaction with Lithium Mist in Light Ion Beam Driven Fusion Reactor Cavities

R.R. Peterson

Fusion Technology Institute
University of Wisconsin
1500 Engineering Drive
Madison, WI 53706

http://fti.neep.wisc.edu

August 1983 (revised March 1984)

UWFDM-536

FIREBALL INTERACTION WITH LITHIUM MIST IN LIGHT ION BEAM DRIVEN FUSION REACTOR CAVITIES

R.R. Peterson

Fusion Engineering Program
Nuclear Engineering Department
University of Wisconsin-Madison
Madison, Wisconsin 53706

August 1983

(Revised)

UWFDM-536

FIREBALL INTERACTION WITH LITHIUM MIST IN LIGHT ION BEAM DRIVEN FUSION REACTOR CAVITIES

R.R. Peterson

Fusion Engineering Program, Nuclear Engineering Department
University of Wisconsin, Madison, Wisconsin 53706

ABSTRACT

The EAGLE (Energy Absorbing Gas, Lithium Ejector) concept has been developed as a method of first wall protection and energy recovery in light ion beam fusion reactors. This concept uses a mist of liquid lithium to cool the target chamber gas between target shots and to protect the first wall from target x-rays and the shock and heat flux of the target generated fireball. The wall protecting nature of this mist is investigated with a one-dimensional Lagrangian multigroup radiation transport hydrodynamics code. Modifications to this code have been made to include the effects of condensation and evaporation of the mist during the propagation of the fireball. Simulations with this code of fireball propagation in EAGLE type reactor cavities have shown that phenomena which may be important to first wall survival are the reflection of the shock off of the mist, the absorption of fireball radiation by the mist and acceleration of mist droplets by the shock.

I. Introduction

The first wall protection cavity gas dynamics problems encountered in light ion beam driven fusion reactor designs are very different from those faced in the design of heavy ion beam and laser driven fusion reactors. The difference occurs because of the cavity gas densities. If propagation of the light ion beams is to be through preformed plasma channels, the density of the gas must be such that the pressure at 0°C is in the range of 1-50 Torr. Self-pinched propagation requires pressures on the order of 1-10 Torr. On the other hand, ballistic propagation of heavy ion beams require less than 10^{-4} Torr and less than 1 Torr (perhaps as low as 10^{-3} Torr) is required for laser propagation. There is the possibility that heavy ion beams could be propagated in the self-pinched mode through 1-10 Torr of gas and a reactor design using such a propagation scheme would have the same potential problems that light ion beam designs encounter.

The distinguishing feature of fusion reactor target chambers containing higher densities of gases is that much of the non-neutronic target energy is absorbed in the gas. The energy, thus absorbed, creates a fireball in the cavity gas which can apply both a wall damaging shock wave and a thermal heat flux to the first wall. Any design of a light ion beam reactor must address the problem of first wall survival under such conditions. The other problem is that it may be difficult to get enough of the target energy out of the cavity gas to allow pumping of the gas and to allow propagation of the beams for the next target shot. A new solution to these problems has been proposed in the recent EPRI sponsored study of technology development planning for light ion beam fusion.

The EAGLE (Energy Absorbing Gas, Lithium Ejector) reactor concept, suggested by the Bechtel group, uses a mist of liquid lithium drops to cool the hot cavity gas. The liquid lithium spray is injected outward from a spray head at the center of the top of the target chamber, downward from the sides of the top and inward from the center of the sides to form a region of mist and cavity gas surrounding a central "core" region of cavity gas alone. The cavity gas, which is xenon, stops most of the fusion target generated x-rays and ions to form a hot fireball in the core region which spreads to the mist region. It has been surmised that the mist will protect the first wall from the shock and heat pulse of the fireball. The purpose of this work is to investigate this conjecture through computer simulation of fireball propagation in EAGLE type reactor cavities.

A schematic picture of the fireball propagation is shown in Fig. 1. In this picture, the basic physical processes present in the EAGLE reactor cavity are depicted. Initially, the soft target x-rays and debris ions are stopped in the core cavity gas while the target neutrons and hard x-rays escape the cavity. This occurs over a time scale on the order of 10^{-7} sec. The energy absorbed in the gas creates a hot fireball which begins to propagate to the first wall. During this phase, the fireball radiates low energy photons, some of which are absorbed by the mist while others reach the first wall, and a shock front is formed. This process continues up until the fireball intersects the mist region at some large fraction of 1 msec. Once the fireball reaches the mist region the shock front is partially reflected and is further attenuated by the conversion of its kinetic energy into vaporizing the lithium drops. The effectiveness of this last mechanism is dependent upon how much vaporization has already occurred because of the earlier absorption of the low

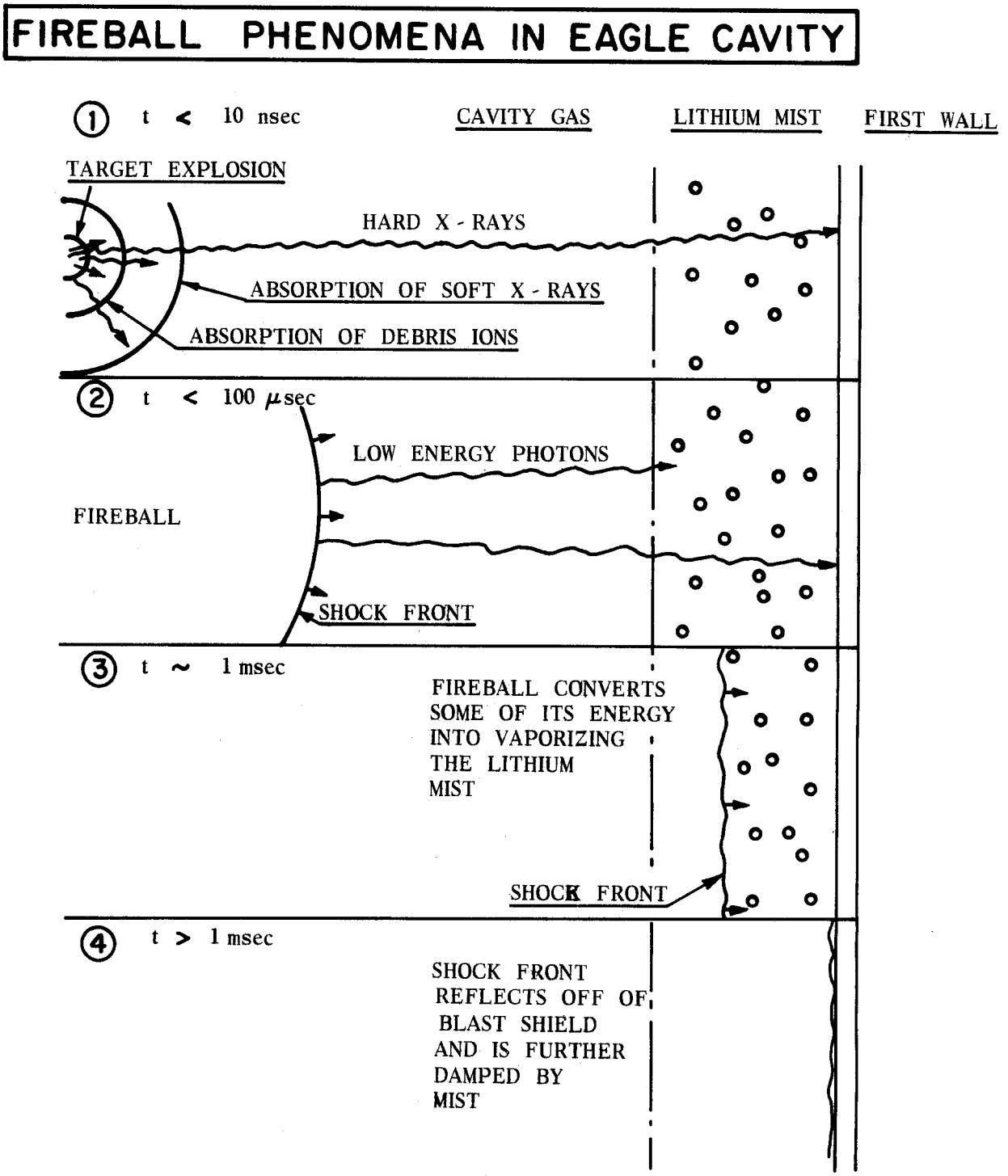

Figure 1. Schematic Picture of Fireball Propagation in EAGLE Reactor Target Chamber.

energy photons. Eventually the shock will reflect off of the first wall, possibly to be further attenuated in the mist.

The discussion that follows begins with a brief description of the modifications that were needed to the computer codes that model these phenomena. The results of simulations are then presented for several cases. These cases include the ETR (1.9 m wall radius, 0.5 m thick mist region) and the DEMO (4 m wall radius, 1 m thick mist region). The ETR would be the first device where the target, driver and reactor cavity are integrated into a single unit, while the DEMO would be the first installation to contain all of the components needed in a commercial light ion beam fusion power plant. Results will be presented for the ETR with variable vaporization rates to determine the sensitivity of the results to lithium drop sizes. Also discussed are results of a simulation for the case where the ETR is close to a "cyclic steady state." Then shown are the results of some simulations of the fireball phenomena up to the point where the shocks intersects the mist/core interface which show, among other things, that the x-ray fluences on the beam transport tubes are not excessively large. Some conclusions and recommendations follow.

II. Computer Modeling

A system of computer codes has been developed at the University of Wisconsin specifically to simulate the propagation of fireballs in such cavity gas [1-4]. A diagram showing this system of codes in shown in Fig. 2. Target x-ray spectra and debris ion energies are provided by the Lagrangian hydrodynamic-thermonuclear burn code, PHD. Equations of state and multi-frequency opacities are provided by the code MIXERG in a form which is readable by the fireball simulation code, FIREMF. This simulation code has Lagrangian hydrodynamics and multi-frequency radiation transport.

Figure 2. Computer Codes Developed at the University of Wisconsin for ICF First Wall Analysis.

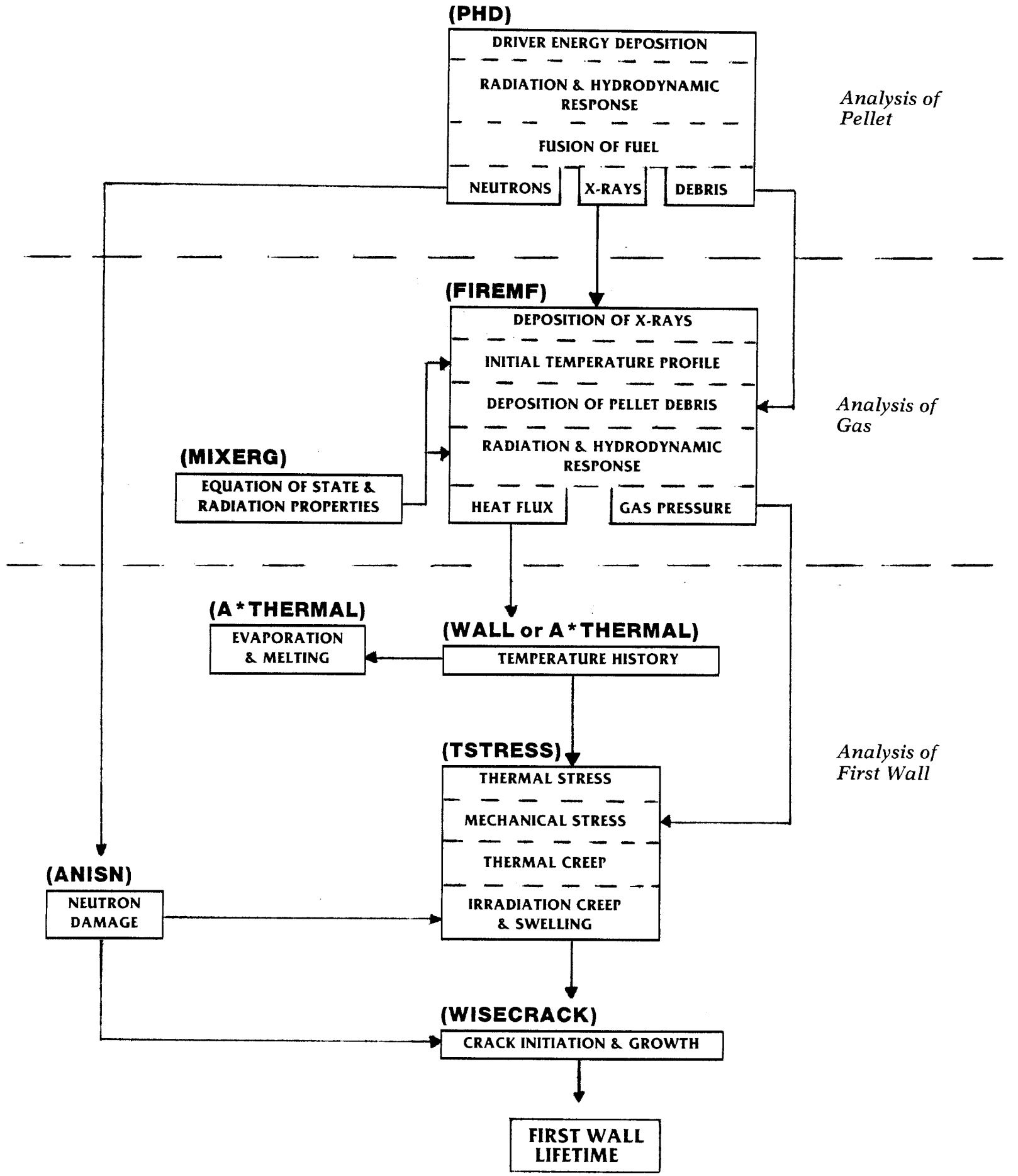

In order to analyze fireball propagation in EAGLE type reactor target chambers, some code development had to be carried out on MIXERG and FIREMF. MIXERG has been modified to include the effects of vaporization on the equations of state and opacities of the cavity gas and lithium mist.

A very simple model has been used for the vaporization: the fraction of lithium which is vaporized is assumed to vary linearly with gas temperature. Specifically, the internal energy density of the gas and mist has now components due to ionization, kinetic energy and vaporization, where the energy density due to vaporization may be written as

$$\begin{aligned} \varepsilon_{vap} &= 0 && \text{if } T_{gas} \leq T_{vap} \\ &= \Delta H \frac{(T_{gas} - T_{vap})}{\Delta T_{vap}} && \text{if } T_{vap} \leq T_{gas} < T_{vap} + \Delta T_{vap} \\ &= \Delta H && \text{if } T_{gas} \geq T_{vap} + \Delta T_{vap} . \end{aligned} \tag{1}$$

T_{gas} and T_{vap} are the gas and vaporization temperatures and ΔH is the heat of vaporization [5],

$$\Delta H = 1.9 \times 10^4 \text{ J/gm} \times \text{mass fraction of Li} . \tag{2}$$

ΔT_{vap} is a parameter which is varied between 0.02 eV and 0.2 eV (T_{vap} = 0.14 eV) to account for the time it takes drops of differing sizes to vaporize.

The opacity of the gas and mist is greatly affected by the vaporization of liquid lithium. In liquid lithium, the atoms are close enough together that they share outer electrons and the liquid becomes a metal. As in all

metals, these shared electrons are arranged in partially filled energy bands where each electron can absorb low energy photons. Thus, photons with less than the photo-ionization energy are easily absorbed while they would not be by the same number of single neutral atoms. Therefore, even though the photo-ionization cross section for xenon is higher than that of lithium, liquid lithium absorbs low energy photons more strongly. The opacity calculation in MIXERG has been modified under the assumptions that the contribution of xenon to the opacity is independent of the presence of lithium, that the contribution of lithium vapor to the opacity is proportional to the vaporized lithium density and that the contribution of the lithium drops is equal to the drop cross-sectional area times the density of drops. If all of the lithium is in the form of drops, the contribution of the lithium to the opacity is

$$\alpha_L = \frac{0.75\ n_{Li}}{r_{drop}\ n_{liq\ Li}}\ , \tag{3}$$

where n_{Li} is Li particle density averaged over a unit volume containing many drops, r_{drop} is the radius of a drop and $n_{liq\ Li}$ is the density of liquid lithium. In this context, opacity is a measure of a material's ability to absorb photons in units of cross section per unit mass.

FIREMF has been modified to include the effect of vaporization on the hydrodynamic pressure. It has been assumed that the drops of liquid lithium do not contribute to the pressure and that xenon gas and lithium vapor are in local thermodynamic equilibrium. Thus the hydrodynamic pressure is just

$$P = n_{Xe}\ T_{gas} + n_{Li\ vapor}\ T_{gas}\ , \tag{4}$$

where $n_{Li\ vapor}$ is the density of Li vapor predicted by the simple vaporization model in MIXERG and n_{Xe} is the particle density of the xenon gas.

Equations of state and opacities calculated by the modified version of MIXERG are shown in Figs. 3, 4 and 5. The internal energy density, which is the sum of the thermal, atomic and ionizational energy per unit mass, is shown in Fig. 3 plotted against gas temperature and gas density for vaporizing liquid lithium mixed with 2.2% xenon by volume. ΔT_{vap} was taken as 0.02 eV. One should notice the sharp rise in energy density at low gas temperature due to the small ΔT_{vap}. In Fig. 4, the same thing is plotted for the case when ΔT_{vap} = 0.2 eV. Notice here the much slower rise at low temperature. This comparison shows how an attempt to model the effect of slower vaporization from larger drops has been made. As a fireball intersects the mist, the temperature increases rapidly so that slower vaporization from large drops means that the vaporization is spread over a wider range of temperatures. Since our system of codes requires time-independent equations of state and since the physics of vaporization of drops is not directly coupled in, it was felt that this was a way of testing the effect of drop size and still staying within the time and resource constraints imposed by the project. The opacity calculated by MIXERG is shown in Fig. 5 for vaporizing lithium with 2.2% xenon for ΔT_{vap} = 0.02 eV and a total density of 2.7×10^{19} cm^{-3}. Here the opacity is plotted against photon energy for two gas temperatures. Notice that, at low temperature, the low and high energy photons are not as greatly absorbed by the gas as are photons with energies between 10 eV and 100 eV. However, at higher gas temperatures the lithium vapor then present will very effectively stop low energy photons. This is because the gas temperature is high enough that there are many singly and multiply ionized lithium atoms present. There

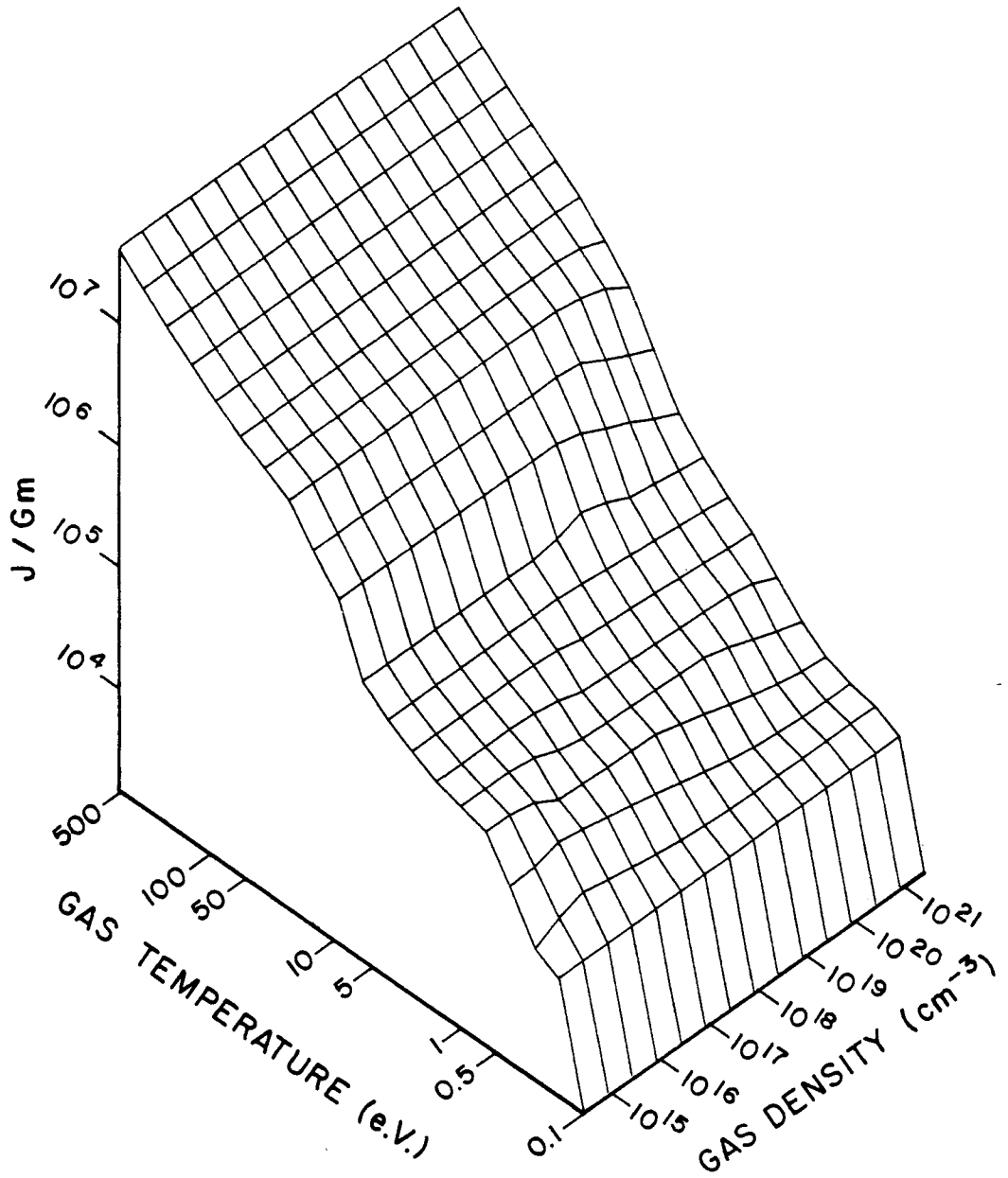

INTERNAL ENERGY DENSITY
0.022 Xe + VAPORIZING Li

T_{vap} = 0.14 eV
ΔT_{vap} = .02 eV

Figure 3. Internal Energy Density Versus Gas Temperature and Density for Vaporizing Liquid Lithium with 2.2% Xenon. ΔT_{vap} = 0.02 eV.

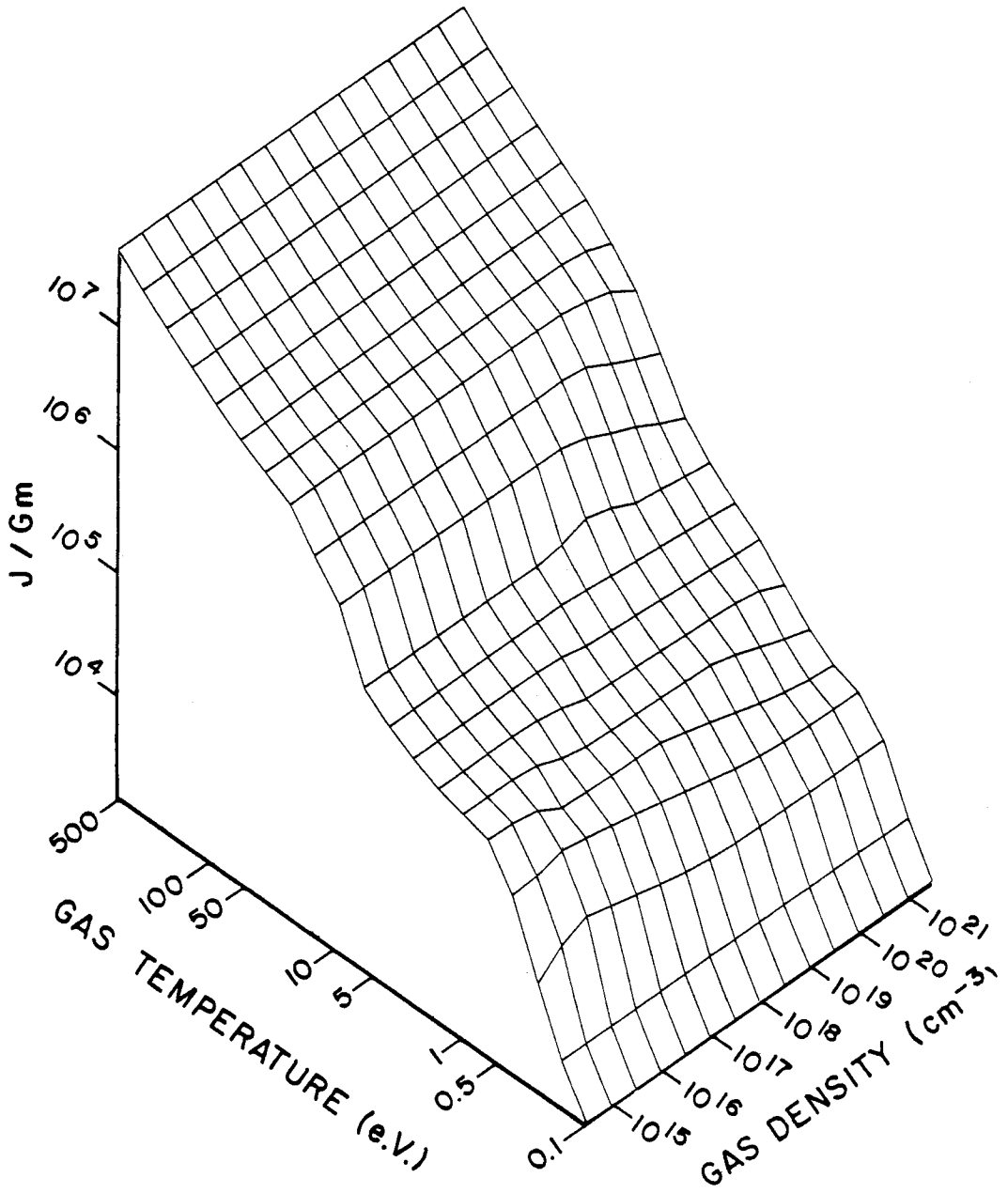

INTERNAL ENERGY DENSITY
0.022 Xe + VAPORIZING Li

T_{vap} = 0.14 eV
ΔT_{vap} = 0.2 eV

Figure 4. Internal Energy Density Versus Gas Temperature and Density for Vaporizing Liquid Lithium with 2.2% Xenon. ΔT_{vap} = 0.2 eV.

Figure 5. Rosseland Opacity for Vaporizing Liquid Lithium and 2.2% Xenon Versus Photon Energy for Gas Temperatures of 0.1 eV and 8.85 eV. The Total Density of Atoms is 2.7×10^{19} cm^{-3}.

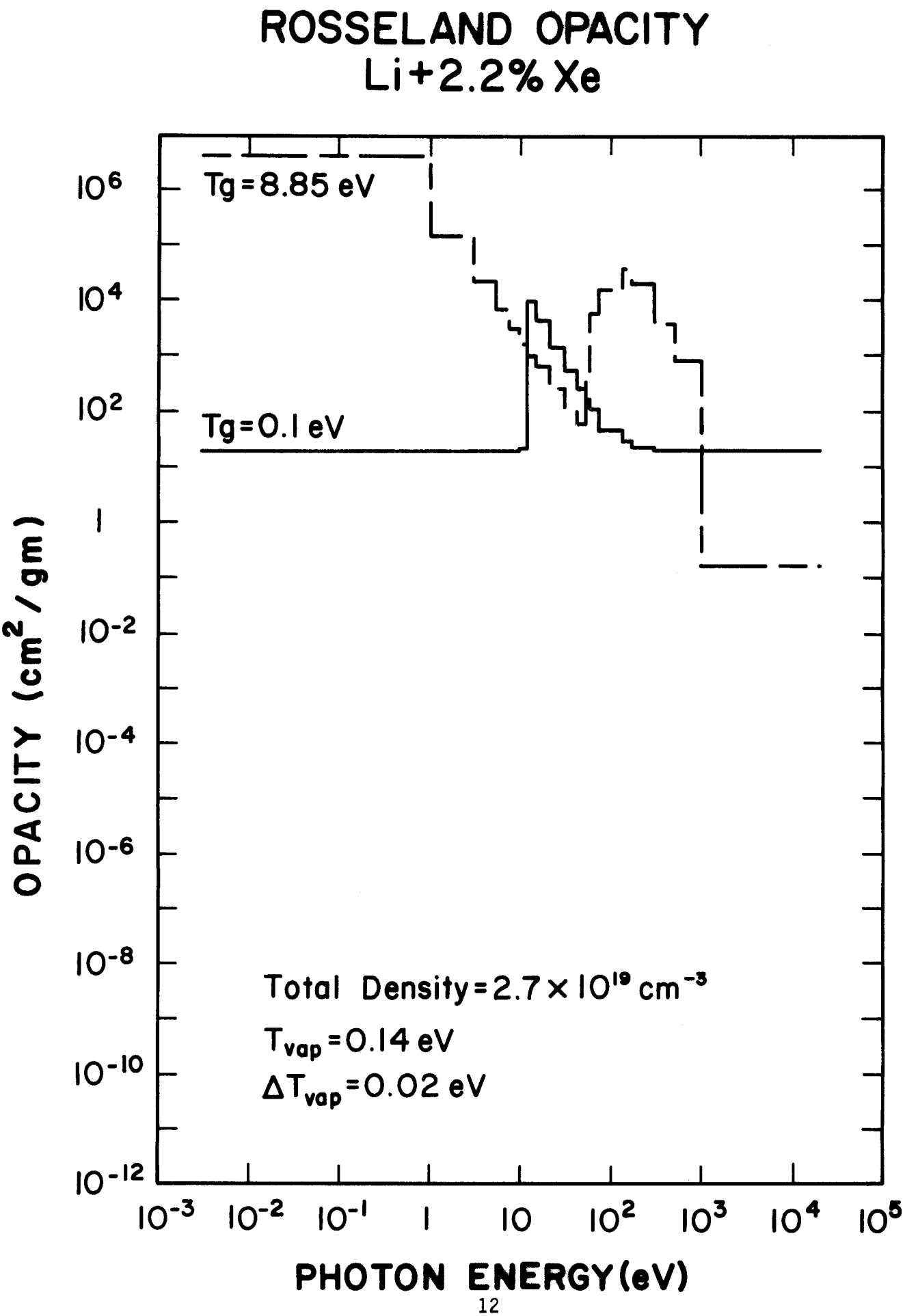

are many free electrons present and the atoms may absorb photons of low energy because the atoms populate many of the excited states and the energy difference between excited atomic states is much lower than the ionization potential. In Fig. 6, the same opacity is plotted for a case where the absorption by lithium drops has been set to zero. Notice that the opacity at low photon energies and low temperatures is more than twelve orders of magnitude lower. This shows that absorption by drops is very important when they are present. Naturally, there is no effect on the opacity at high temperature.

III. Results

The codes described in the previous section have been used to simulate fireball phenomena in EAGLE type reactor cavities. Results for the whole cavity gas, with both core and mist regions, are compiled in Table 1 for several cavity conditions. The response of the core gas by itself is summarized in Table 2 for core gases with and without lithium vapor and for both the ETR and DEMO. The details of these calculations are presented in the remainder of this section.

The ETR and the DEMO are devices which are parts of a research and development plan for light ion beam fusion sponsored by the Electric Power Research Institute (EPRI). This study was completed in late 1983 and an EPRI report describing the plan should be available soon. The Engineering Test Reactor (ETR) would be the first facility to integrate the target, ion beam and reactor and its primary goal would be to demonstrate that this integration is possible. The DEMO is a demonstration reactor which would be the first light ion fusion facility that includes all of the systems and components required by a commercial power plant and its goal is to establish the commercial

TABLE 1. Fireball Results

Design	ETR	DEMO	ETR	ETR
Mode	1 shot	1 shot	steady state	1 shot
ΔT_{vap} (eV)	0.02	0.02	0.02	0.2
Target Yield (MJ)	30	300	30	30
Max. Pressure on Wall (atm)	2.3	4.0	1.9	2.6
Initial Fireball Energy (MJ)	8.01	80.4	8.01	8.01
Energy Radiated to Wall (MJ)	1.11	2.17	3.21	0.95
Radiant Energy Density on Wall (J/cm^2)	2.4	1.1	7.1	2.1

TABLE 2. Fireball Results at Core/Mist Interface

Design	ETR	ETR	DEMO	DEMO
Target Yield (MJ)	30	30	300	300
Xenon Density (cm^{-3})	2.12×10^{17}	2.12×10^{17}	2.12×10^{17}	2.12×10^{17}
Lithium Density (cm^{-3})	3.12×10^{17}	0	3.12×10^{17}	0
X-Ray Fluence on Interface (J/cm^2)	0.688	0.780	2.97	3.02
Energy Density Radiated to Mist by Time of Arrival of Shock (J/cm^2)	1.77	18	0.27	44
Total Energy Radiated to Mist by Time of Arrival of Shock (MJ)	0.435	4.5	0.31	50
Shock Pressure at Interface (atm)	~ 2	~ 1	~ 2	~ 1

Figure 6. Rosseland Opacity for Vaporizing Lithium and 2.2% Xenon Versus Photon Energy for Gas Temperatures of 0.1 eV and 8.85 eV. The Total Density of Atoms is 2.7×10^{19} cm^{-3} and the Contribution of Liquid Lithium Drops to the Opacity has been Neglected.

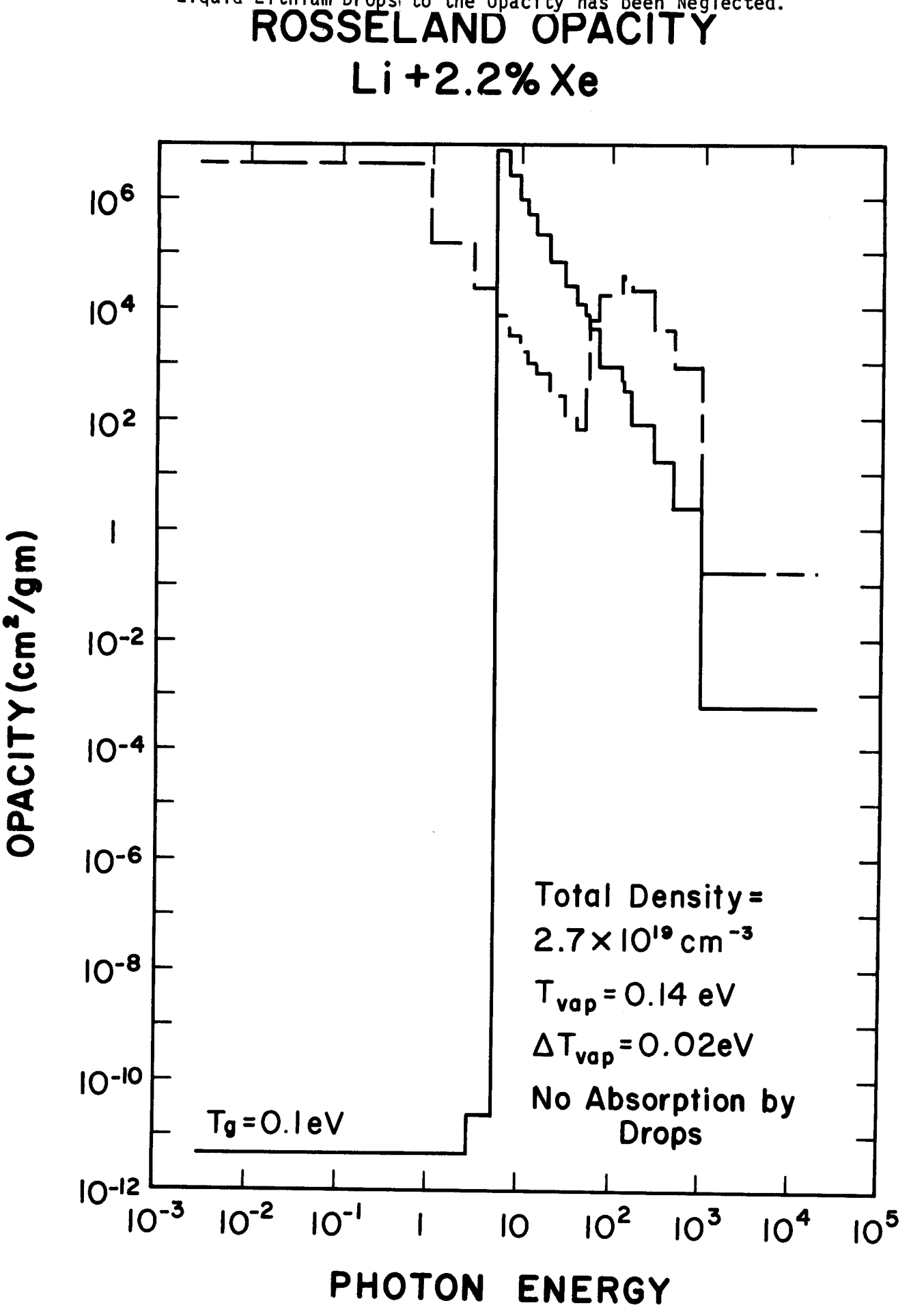

feasibility of light ion fusion. The two designs have similar designs for their target explosion chambers but the dimensions are different: both are right circular cylinders but the ETR is 1.9 m in radius with a 0.5 m thick mist region while the DEMO is 4.0 m in radius with a 1.0 m thick mist. As pointed out in Tables 1 and 2, the target yield is 30 MJ in the ETR and 300 MJ in the DEMO.

A. Target Output Spectrum

Since the opacities and x-ray stopping powers of the gas and vapor are dependent upon photon energy, it is necessary to know the spectrum of x-rays coming out of the target. We have used the PHD thermonuclear burn code to do this for the single-shell multi-layered target shown in Fig. 7. This is the same target design used by the University of Wisconsin in the HIBALL reactor study [6]. This target is based on an ion beam target design which appeared in the open literature [7]. There is some inconsistency with this target, which was designed for a heavy ion beam driver, because it has a thick lead layer on the outside. It is assumed that the spectrum for a properly designed light ion beam target will not be radically different than that which was calculated using this target design.

The spectrum is shown in Fig. 8. This is the spectrum integrated out to 3.5 nsec. Notice that the spectrum consists of two components; one soft component centered around 1 keV, the other harder component around 100 keV. The soft component contains most of the energy and is most important to cavity considerations. The hard component has a much longer stopping length in the cavity gases and materials and has very little effect on either the fireball dynamics or the lifetimes of the reactor components. The total energy in target x-rays and debris ions is 27% of the total yield. Of this 27%, 20% is

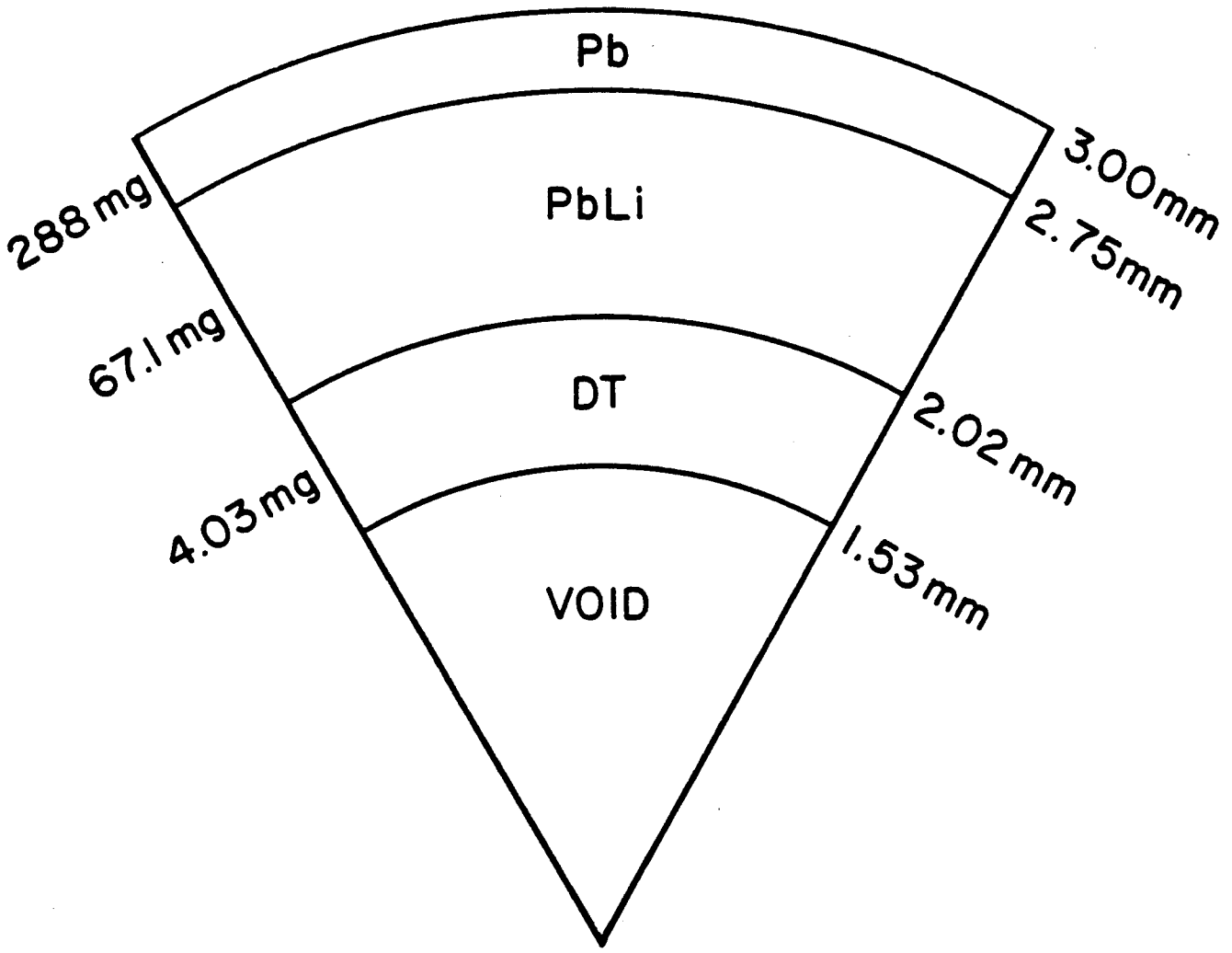

Figure 7. HIBALL Target Design.

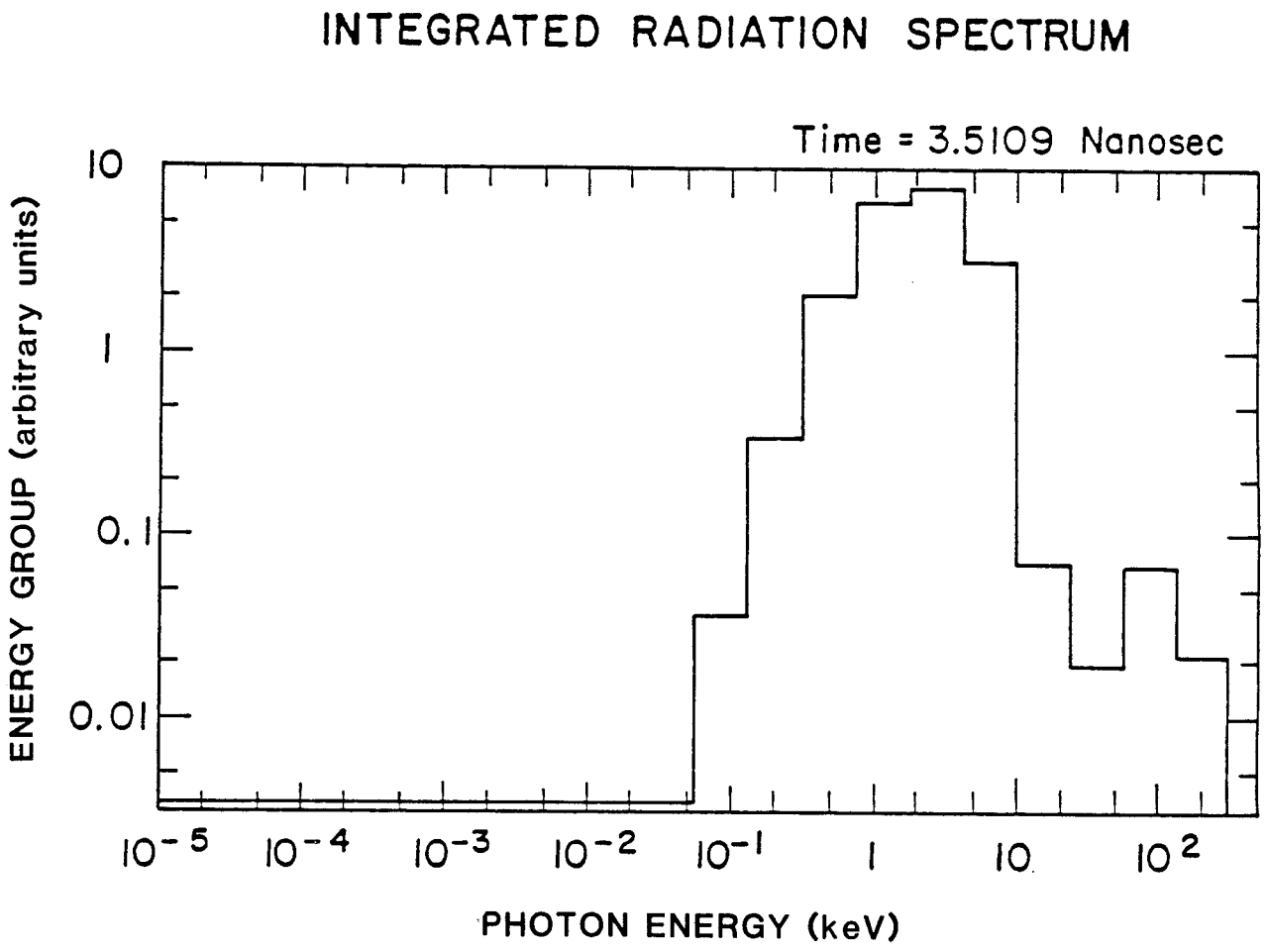

Figure 8. Target X-Ray Spectrum for HIBALL Target as Calculated with PHD Integrated Out to 3.5 nsec.

in x-rays and 7% is in debris. The debris ions are stopped in a very short distance in the target explosion chamber gas and contribute their energy to the initial heating of the central fireball. This spectrum is an input into the fireball simulation calculations.

B. ETR Base Case

Fireball phenomena inside the cavity of the Engineering Test Reactor (ETR) have been simulated with the FIREMF multi-frequency radiative heat transport Lagrangian hydrodynamics code [2]. The ETR target chamber is a right circular cylinder 1.9 m in radius. The cavity gas for the "base case" calculation has an initial temperature of 783°C. The target yield for the ETR is 30 MJ, roughly 8 MJ of which is in the form of x-rays and target debris with the remainder being in neutrons. The core region of the cavity gas has a xenon density of 2.12×10^{17} cm^{-3} (6 torr at 0°C) and a lithium vapor density of 3.13×10^{17} cm^{-3}. The gas in the mist region is cooled somewhat by the mist so that, to have a uniform xenon pressure, the xenon density is increased to 5.25×10^{17} cm^{-3} in the mist region. The total density of lithium, in the mist and vapor phases, is 2.39×10^{19} cm^{-3}.

The results of computer simulation of fireball dynamics in the ETR for this base case are shown in Figs. 9 through 16. Figure 9 shows the positions of the Lagrangian zone boundaries in FIREMF plotted against time. Since Lagrangian zones contain a fixed mass of fluid and move with the fluid, this figure shows the hydrodynamic motion of the cavity gas and mist after the target explosion. The mist region begins at 140 cm where the zone boundaries are spaced more closely together and is driven back towards the first wall and compressed by the fireball. One can see from Fig. 9 that the shock speed is much lower in the mist region, an effect which occurs because the mist

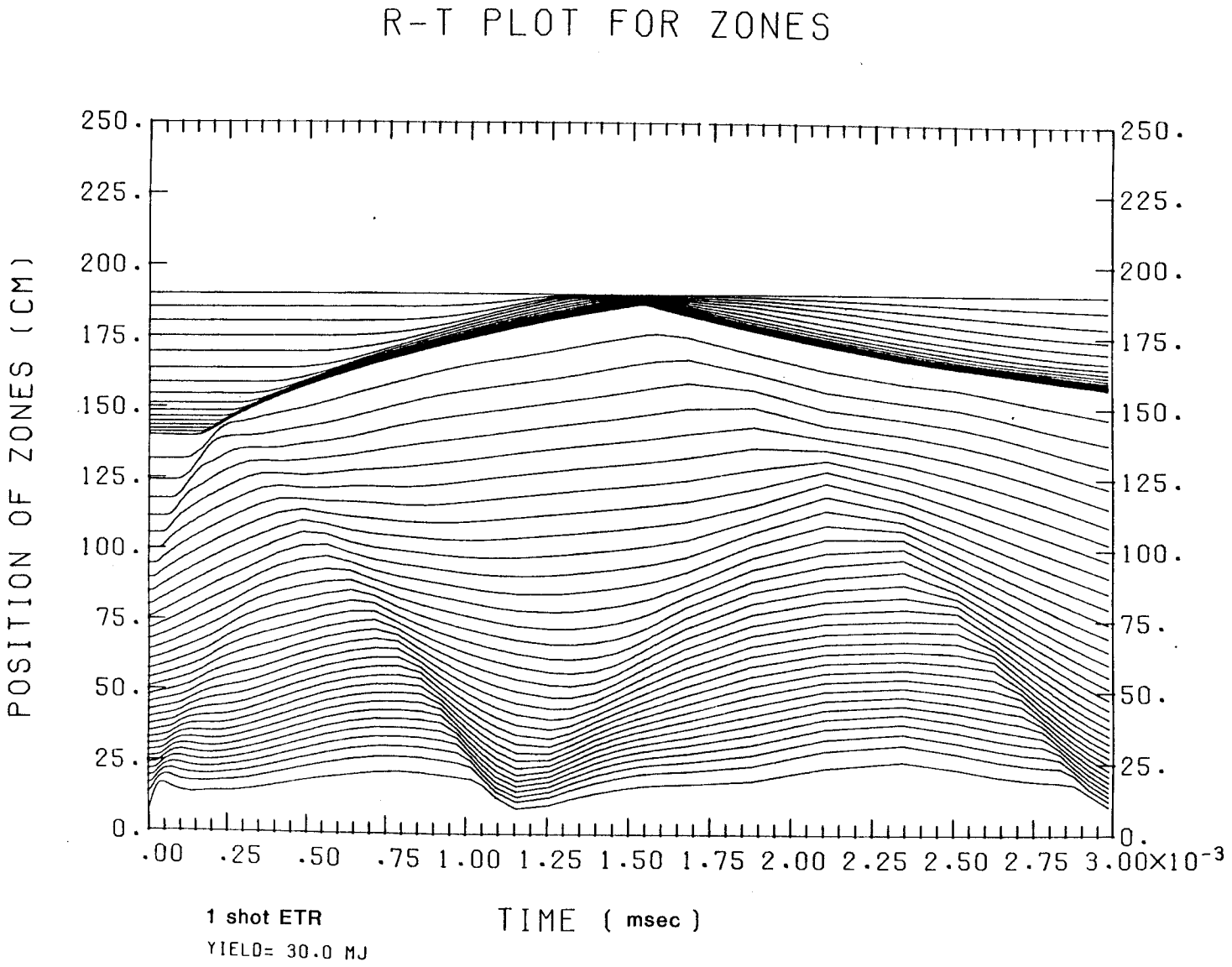

Figure 9. Position of Lagrangian Zone Boundaries Versus Time for ETR Base Case.

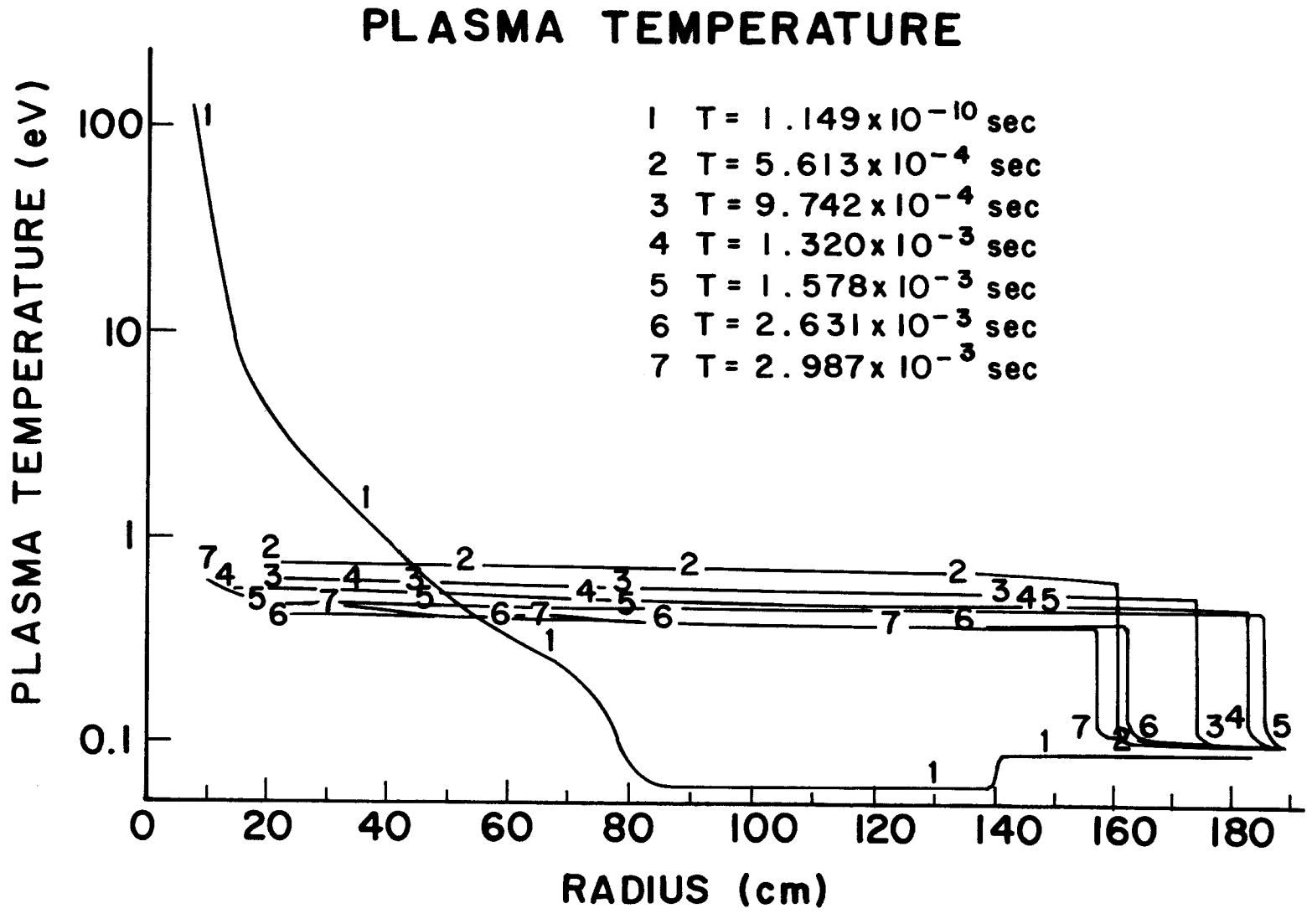

Figure 10. Plasma Temperature Profiles at Various Times for ETR Base Case.

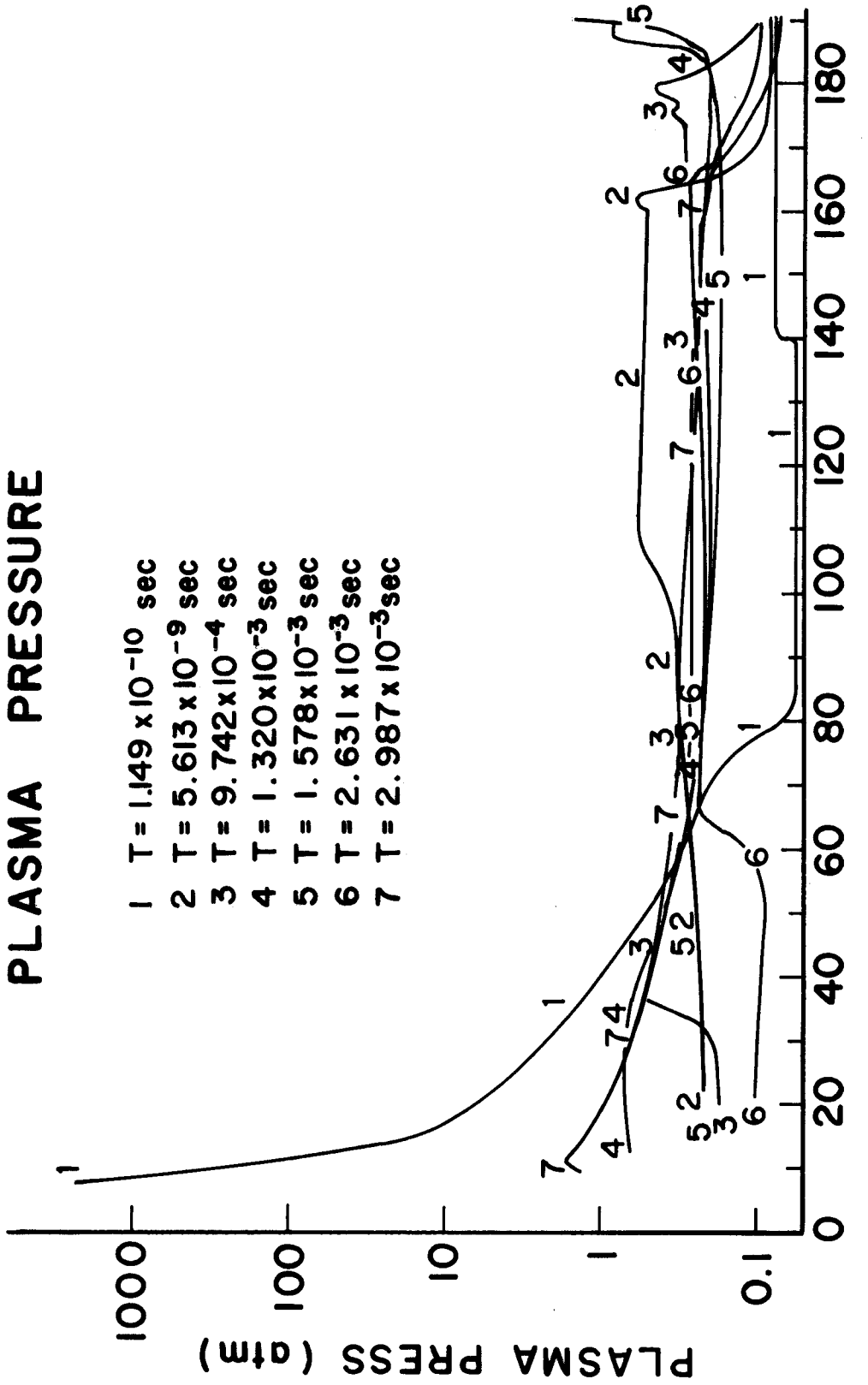

Figure 11. Pressure Profiles at Various Times for ETR Base Case.

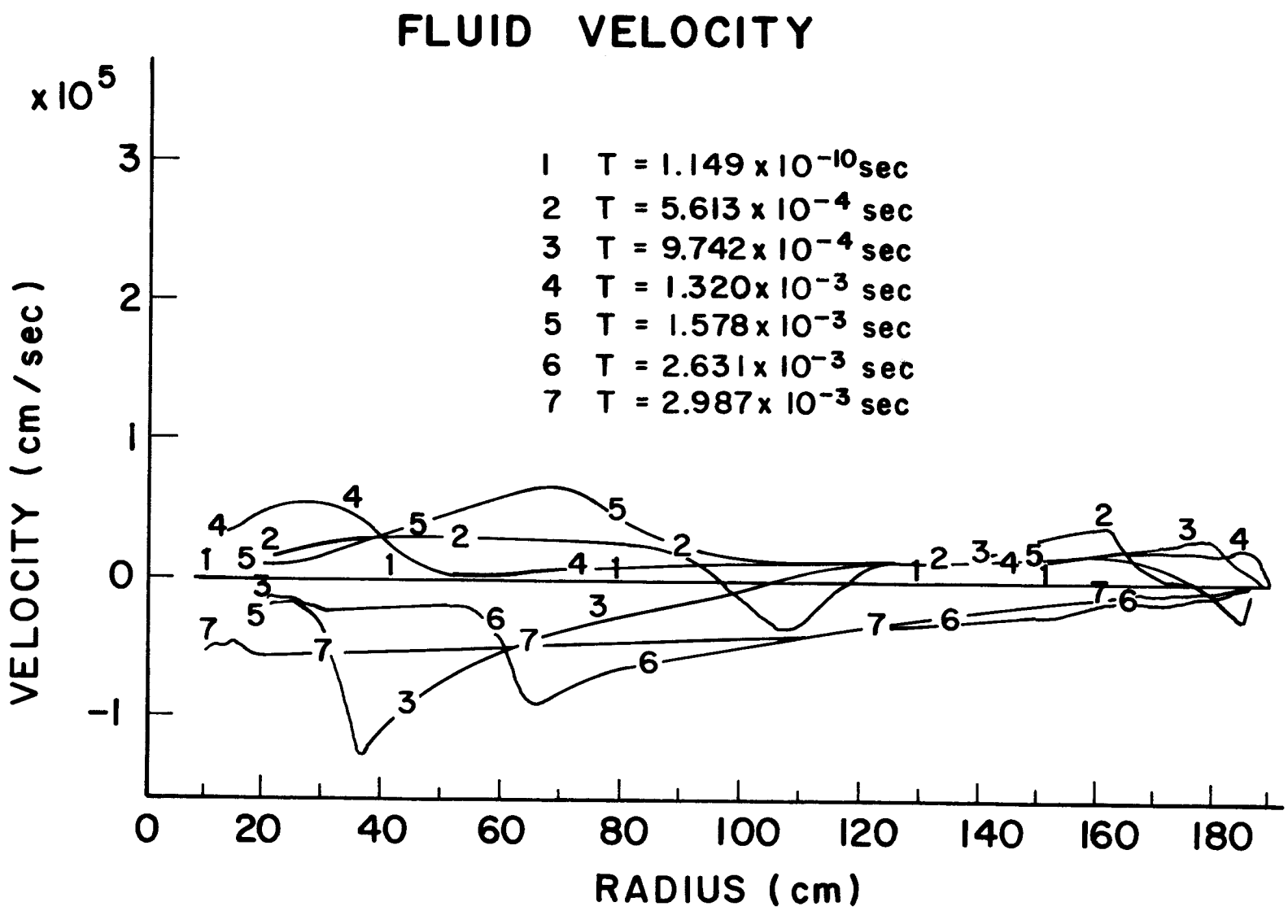

Figure 12. Fluid Velocity Profiles at Various Times for ETR Base Case.

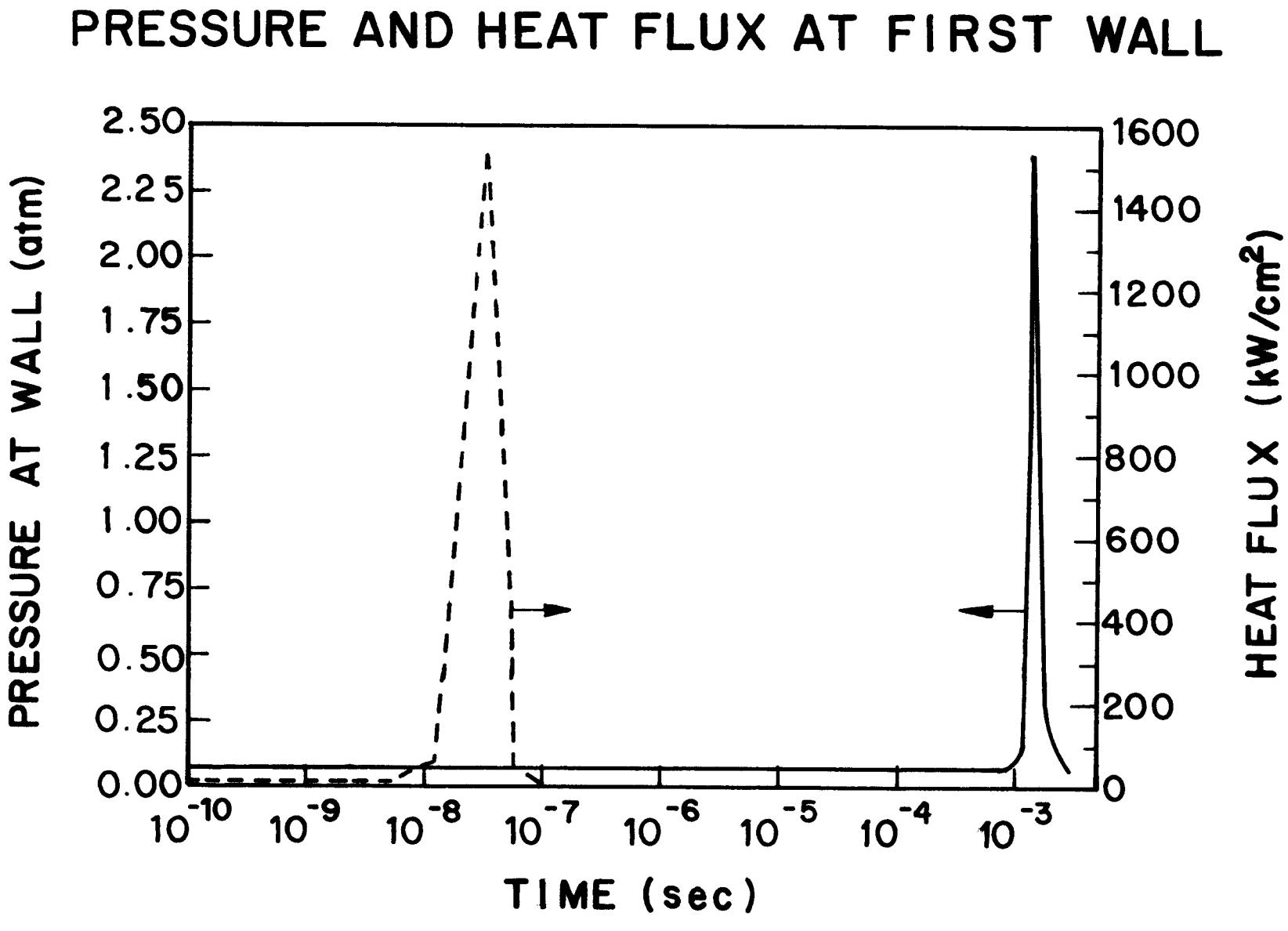

Figure 13. Shock Overpressure and Radiant Heat Flux on Blast Shield of ETR Base Case Versus Time.

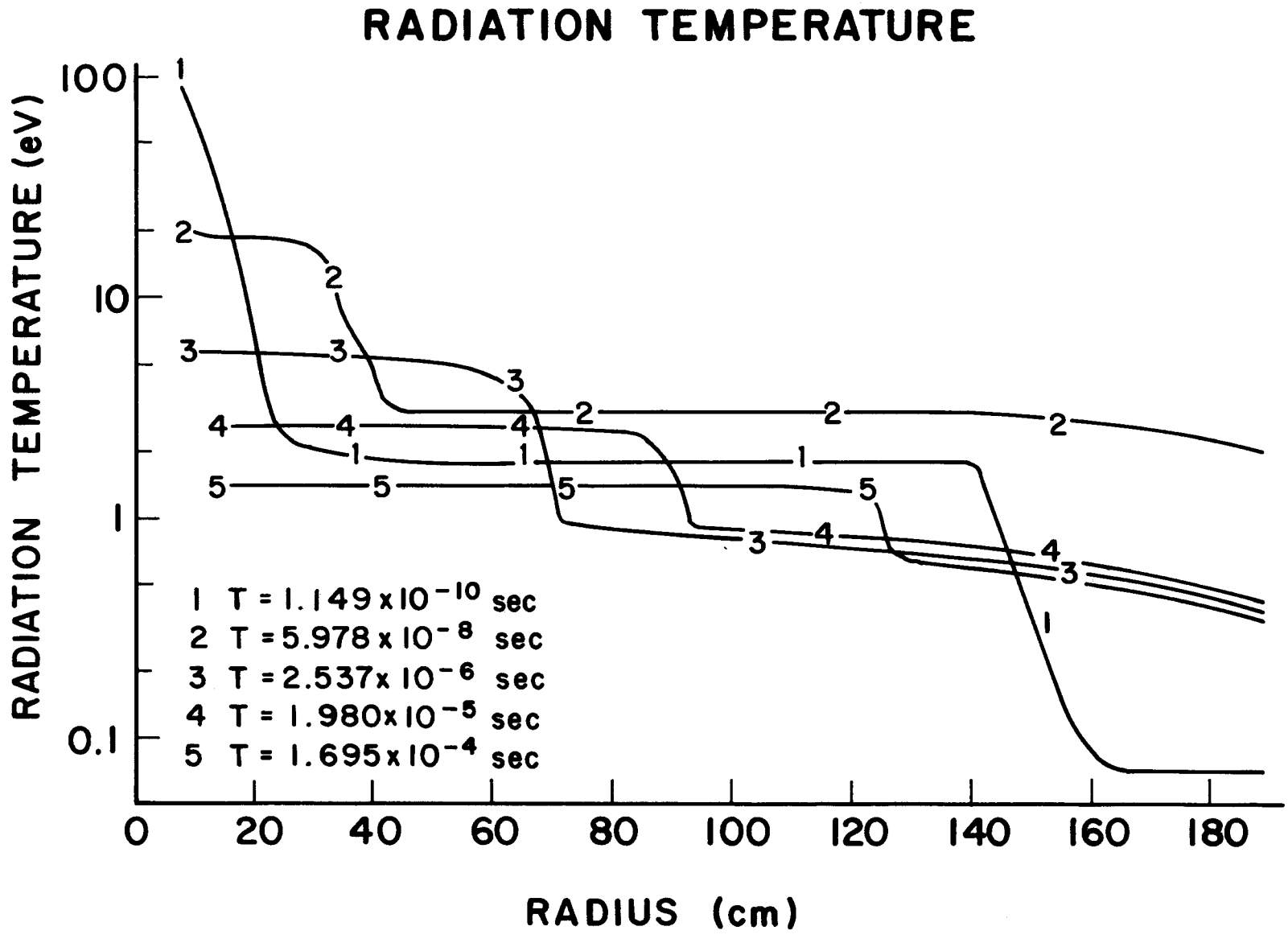

Figure 14. Radiation Temperature Profiles at Various Times for ETR Base Case.

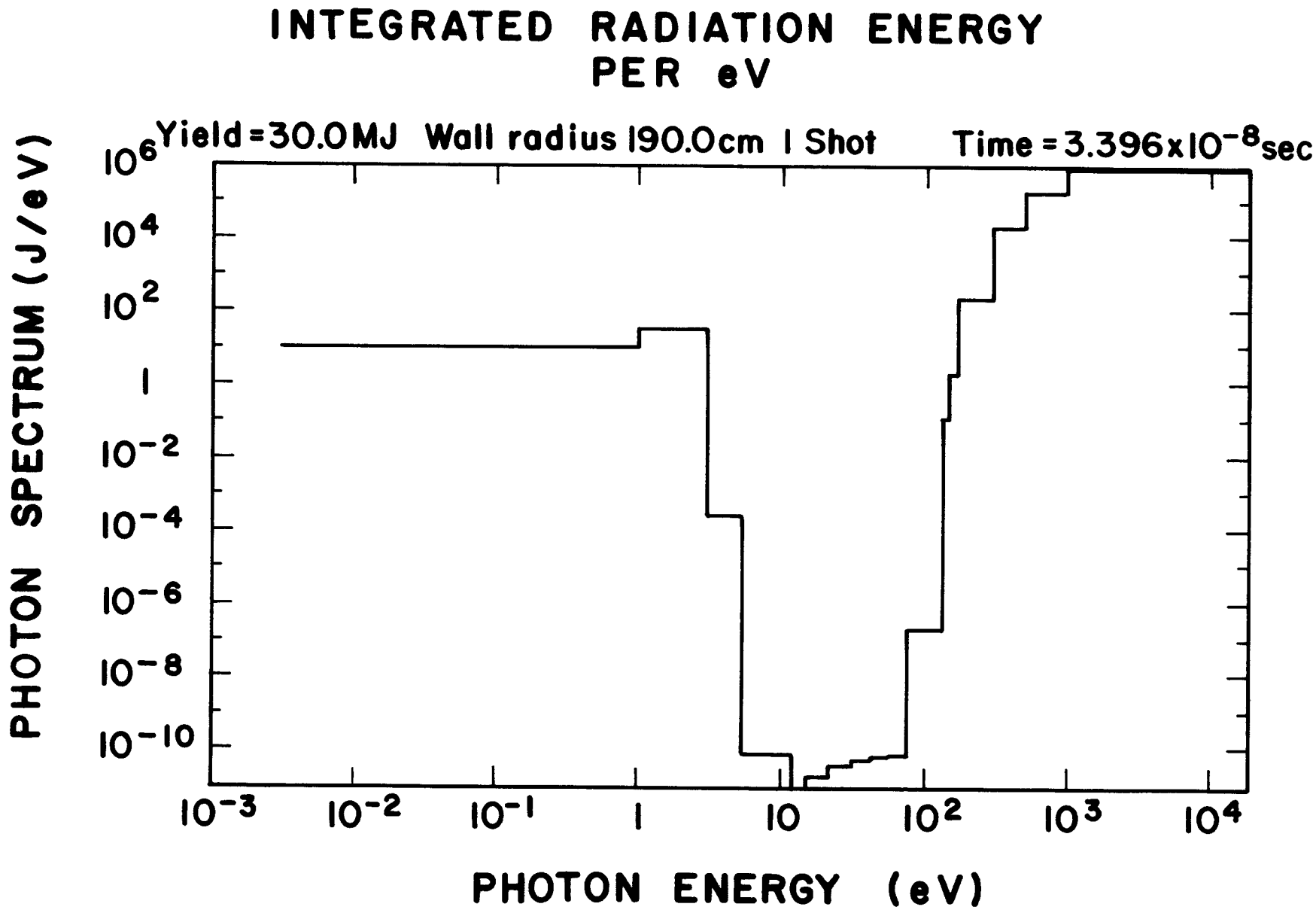

Figure 15. Photon Spectrum at First Wall Integrated out to 3.4×10^{-8} sec for ETR Base Case.

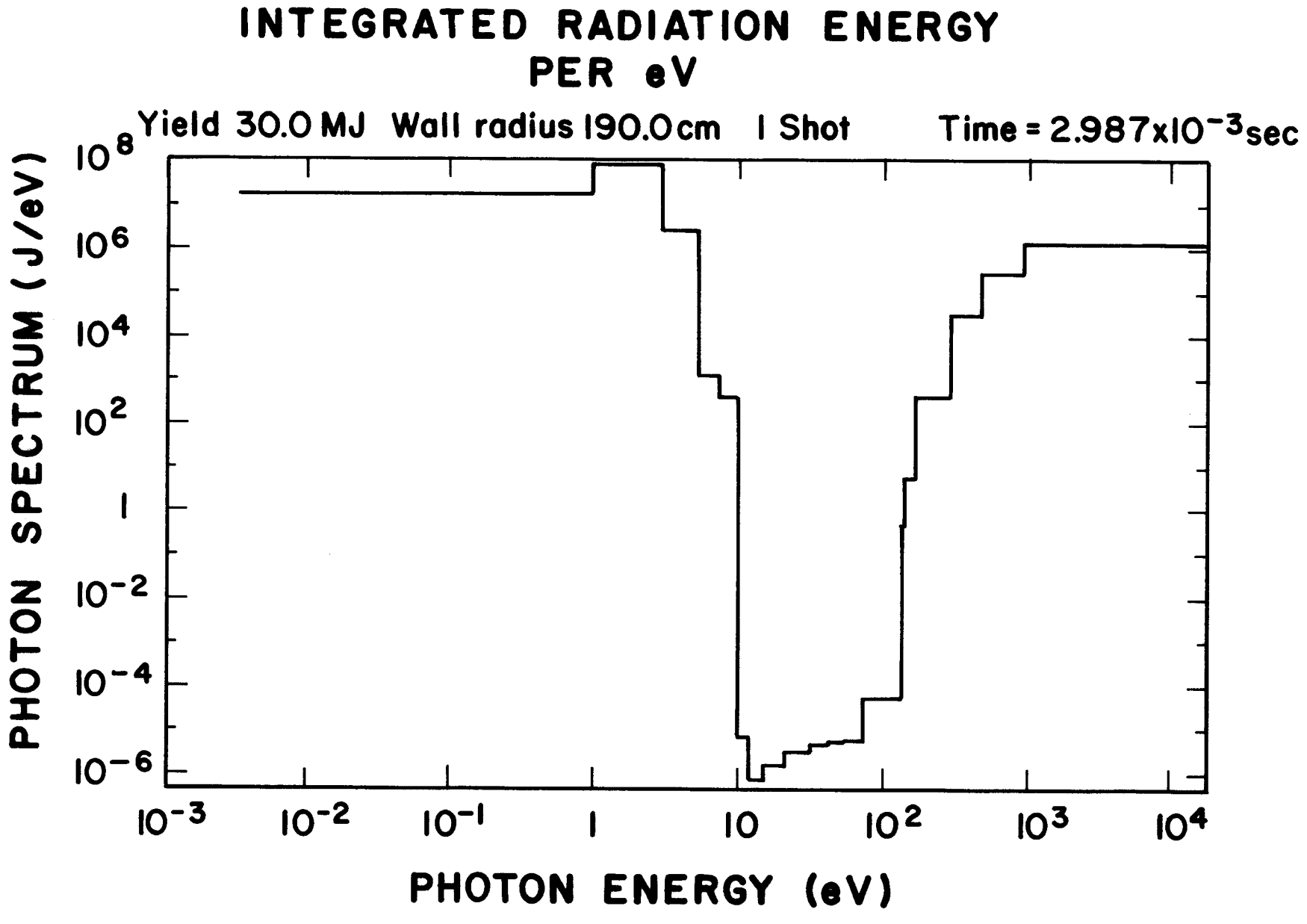

Figure 16. Photon Spectrum at First Wall Integrated Out to 3 x 10^{-3} sec for ETR Base Case.

droplets are assumed to move with the gas so that the mass density that the shock wave experiences in the mist is much higher than in the core region. This density discontinuity results in a reflection of the shock off of the interface between the core and the mist regions which can be seen in Fig. 9. The hydrodynamic motion early in time shows that there are two shocks which are launched initially. This can be explained by the plasma temperature profile shown in Fig. 10. One can see that at a very early time the plasma temperature profile has two places where there is a sharp drop. This is due to the target x-ray deposition profile. The pressure profiles are shown in Fig. 11, where related sharp drops in the pressure can be seen at the early time. It is this early pressure profile which launches the two shocks seen in Fig. 9. Another way of looking at the hydrodynamic motion is through the fluid velocity, plotted against position for different times after the micro-explosion in Fig. 12. One can see here that the fluid velocity in the mist is as high as 3×10^4 cm/sec while it is as much as two times higher in the core. At 0.56 msec, a reflected shock can be seen with its negative velocity of 4×10^4 cm/sec at 110 cm while the shock in the mist can be seen at the same time at 160 cm with its velocity of 3×10^4 cm/sec. At 0.97 msec the reflected shock is only 35 cm from the cavity center and has a velocity of 1.3×10^5 cm/sec while the transmitted shock is at 180 cm and only has a velocity of 2×10^4 cm/sec. This is because, just before the shock reaches the wall at 1.5 msec, the density is greatly increased in the mist region as the shock compresses it up against the wall while the density in the core is reduced because the initial shocks have rarified the region. One potential problem that Fig. 12 brings to light is the possibility of accelerating drops of lithium up to about 10^4 cm/sec through entrainment by the shock which could lead to

erosion of the wall. The hydrodynamic shock wave in the mist results in an overpressure on the first wall, shown plotted against time in Fig. 13. The maximum pressure on the wall is 2.3 atmospheres.

In addition to the effects of pressure on the wall, the fireball can damage the first wall with a thermal radiation flux. Plotted along with the pressure in Fig. 13, this radiation flux has a very high, very short pulse. Radiation temperature, which is proportional to the fourth root of the radiant energy flux, has profiles plotted for a few early times in Fig. 14. This figure shows that, at 0.6×10^{-7} sec after the microexplosion of the target, the radiation temperature near the wall has reached the relatively high value of about 2 eV, which translates into a heat flux of 1.6×10^{6} W/cm^2. It can be noted that there is a gradual decline in the radiation temperature in moving from the core/mist interface to the first wall. This is due to absorption by the lithium drops. At the later times, the radiation temperature drops to about 0.4 eV which means a three order of magnitude reduction in the heat fluxes to 2×10^{3} W/cm^2. This reduction in the radiative heat flux on the first wall is due mainly to a decrease in the central fireball temperature by a factor of about 8, with an additional smaller contribution by changes in the opacities by factors of 2 or 3. The spectrum of radiant energy on the first wall is shown in Fig. 15, integrated in time out to 3.4×10^{-8} sec, and in Fig. 16, integrated out to 3×10^{-3} sec. These two plots show that the early heat flux contains relatively hot photons while the late heat flux consists of cooler photons. This is consistent with a 40 fold reduction in the central fireball temperature during the intervening time.

C. DEMO Base Case

The same calculations have been completed for the DEMO. The only differences between the DEMO calculations and those for the ETR base case presented in the preceding section are the yield, which is 300 MJ instead of 30 MJ for the ETR, the wall radius, which is 4 m, and the width of the mist region, which is 1 m.

Many of the results for the DEMO base case are qualitatively similar to the results for the ETR base case and they will not be presented in detail. The one thing that is different is the radiation temperature profile, shown in Fig. 17. There is a much greater attenuation of the radiation flux in the mist region because the mist region is thicker. In the DEMO, the radiation temperature falls by a factor of 3 or more, meaning that the radiation reaching the wall is less than 1% of that leaving the core region. In comparison, the ETR base case shown in Fig. 14 has a reduction in the radiation temperature by a factor of 2 or less, meaning that more than 6% of the radiant energy entering the mist reaches the wall.

D. ETR Steady State Case

When the reactor is operated in a burst mode with many microexplosions in succession, the cavity gas does not initially lose as much energy before the next shot as it gained from the most recent microexplosion. The average temperature of the target chamber gas will increase on each shot until as much energy is lost through radiation, conduction, convection and condensation heat transfer as is gained from the microexplosion. This condition is called the cyclic steady state.

The FIREMF and MIXERG codes have been used to investigate the cyclic steady state for the ETR. The ETR base case calculation described in section

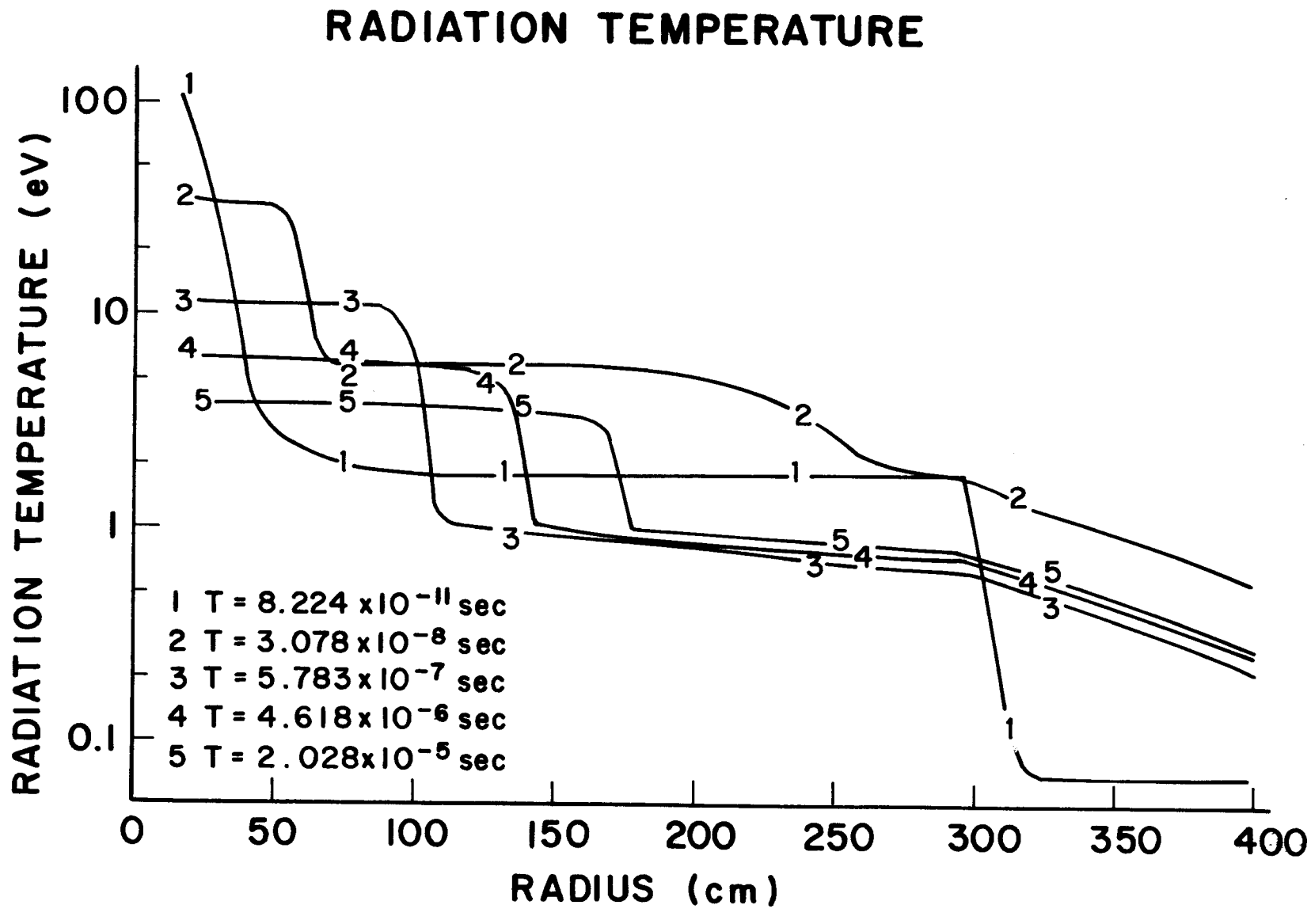

Figure 17. Radiation Temperature Profiles at Various Times for DEMO Base Case.

III.B corresponds to the initial shot in a burst of many shots. The hydrodynamic motion of the gas for this first shot, shown in Fig. 9, indicates that there are shocks reflecting off of the wall, the mist/core interface and the center of the cavity. Since this calculation is one-dimensional, these reflections will not continue as predicted by the code past a few reflections but they probably will lead to mixing of gas and mist into a homogeneous mixture at a roughly uniform temperature. The problem at hand is to determine that uniform gas temperature in the cyclic steady state. The approach used here is to test initial uniform gas temperatures with FIREMF and to compare the radiated and conducted energy with the microexplosion energy deposited in the gas.

The FIREMF code in its present form does not include the energy lost to the surface of the target chamber through condensation of lithium vapor. For this reason, cases where the average gas temperatures just before the next microexplosion are greater than the vaporization temperature of lithium cannot be accurately simulated with this code. If the average gas temperature is higher than the vaporization temperature for close to a second or more, lithium vapor in the cavity will condense on the cool walls of the cavity. Thus, since the repetition rate is on the order of 1 Hz, the gas temperature should not be more than the vaporization temperature. The first guess used to test the steady state condition is the uniform gas temperature equaling the vaporization temperature.

There are two major differences between the calculations where the initial gas temperature is the vaporization temperature and ETR base case: the radiant energy on the first wall is much lower for the base case and the maximum pressure is higher in the base case. The radiant energy on the first

wall is 3.21 MJ when the initial gas temperature is the vaporization temperature while it is 1.11 MJ in the base case. The energy initially in the fireball is 8.01 MJ, which means that since the conduction energy is negligible there must be on the order of 4 to 5 MJ of heat loss from the gas in convection, that is in gas pumped out of the cavity, or in condensation on the surfaces. Condensation on the surfaces includes any sensible heat of lithium drops lost from the cavity through sticking on the surface or by being pumped out in the gas. The pressure pulse on the first wall is 1.9 atm compared with 2.3 atm in the base case. This reduction occurs through a combination of increased pressure outside the fireball and, thus, a reduction in the pressure ratio of the shock, broadening of the shock front by increased radiative heat transfer, and energy loss through radiation which further reduces the shock pressure ratio.

E. Sensitivity of Fireball Propagative to Vaporization Rate

The sensitivity of fireball propagation to the rate of vaporization is very important because of the great difficulty in determining this rate. The difficulty arises because the rate is dependent upon the size of the lithium drops, which cannot be determined easily. The drops may be broken by the shock and there is some range of drop sizes which results from the lithium jets. Parameterization of the problem was attempted with ΔT_{vap} as described in section II.

The sensitivity of the fireball calculations to the vaporization rate is tested by comparing a FIREMF code simulation for the ETR with ΔT_{vap} = 0.2 eV with the ETR base case (ΔT_{vap} = 0.02 eV). The comparison is shown in Table 1. There was roughly a 15% increase in maximum overpressure and a 15% decrease in the energy radiated to the first wall for the case with ΔT_{vap} = 0.2 eV.

Vaporization is slower in this case so there is less energy absorbed from the shock through vaporization. Why the radiant energy on the wall changes is less clear but it may have to do with changes in the opacity of the gas because of vaporization. In any case, the changes in the fireball behavior are not large compared to other uncertainties in the analysis of the target chamber.

F. Target X-Ray Flux and Fireball Effects on Beam Transport Tubes

One possible feature of the EAGLE reactor cavity concept is a system of beam transport tubes for preventing the mist from interfering with the beam transport. These tubes would reach through the mist to the core region from the blast shield. Since these tubes do not have the protection of the mist region, the x-ray fluxes and fireball effects on the inside tips of these tubes must be determined.

The FIREMF code has been used to determine the target x-ray fluences, thermal heat fluxes and shock overpressures on the tip of these transport tubes for the case with an equilibrium lithium vapor density of 3.12×10^{17} cm^{-3} in the core and for the case where there is no lithium vapor. The radiant heat and unattenuated x-ray spectra at the core/mist interface of the ETR are shown in Figs. 18 and 19 for the cases with and without lithium vapor respectively. The spectrum of photons leaving the target is also shown for comparison. In both cases, the spectra contains three components: unattenuated target x-rays, warm photons which emanate from the fireball early in its propagation while it is still hot, and cool photons leaving the fireball later while it is cool. The case where there is no lithium is different mainly in the much higher level of cool fireball photons. This is demonstrated further in Table 2 where results are shown for the core/mist interface for both the

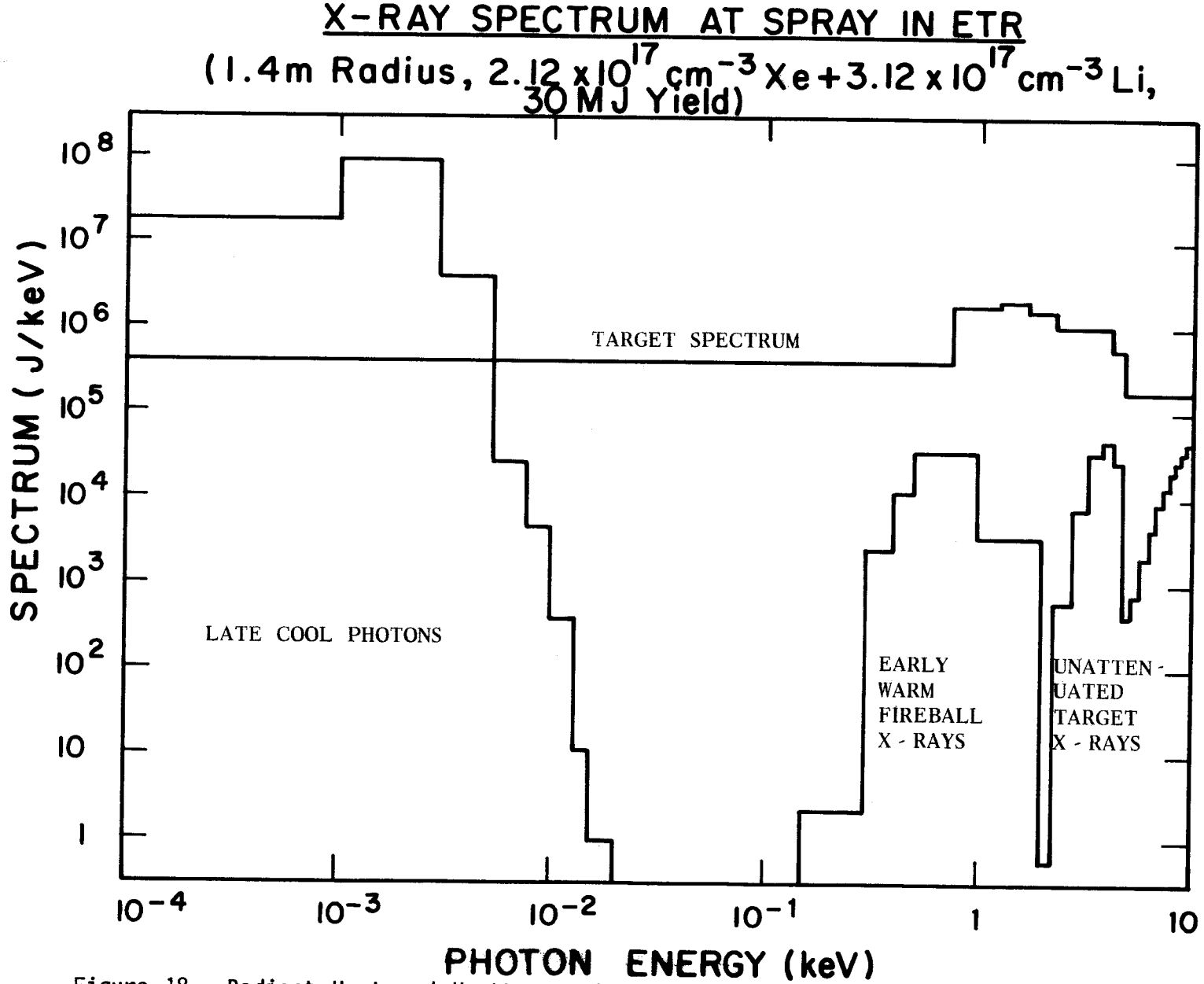

Figure 18. Radiant Heat and Unattenuated Target X-Ray Spectrum at Core/Mist Interface of ETR with 3.12 x 10^{17} cm^{-3} of Lithium Vapor in the Core Integrated in Time. Target Spectrum is Also Shown for Comparison.

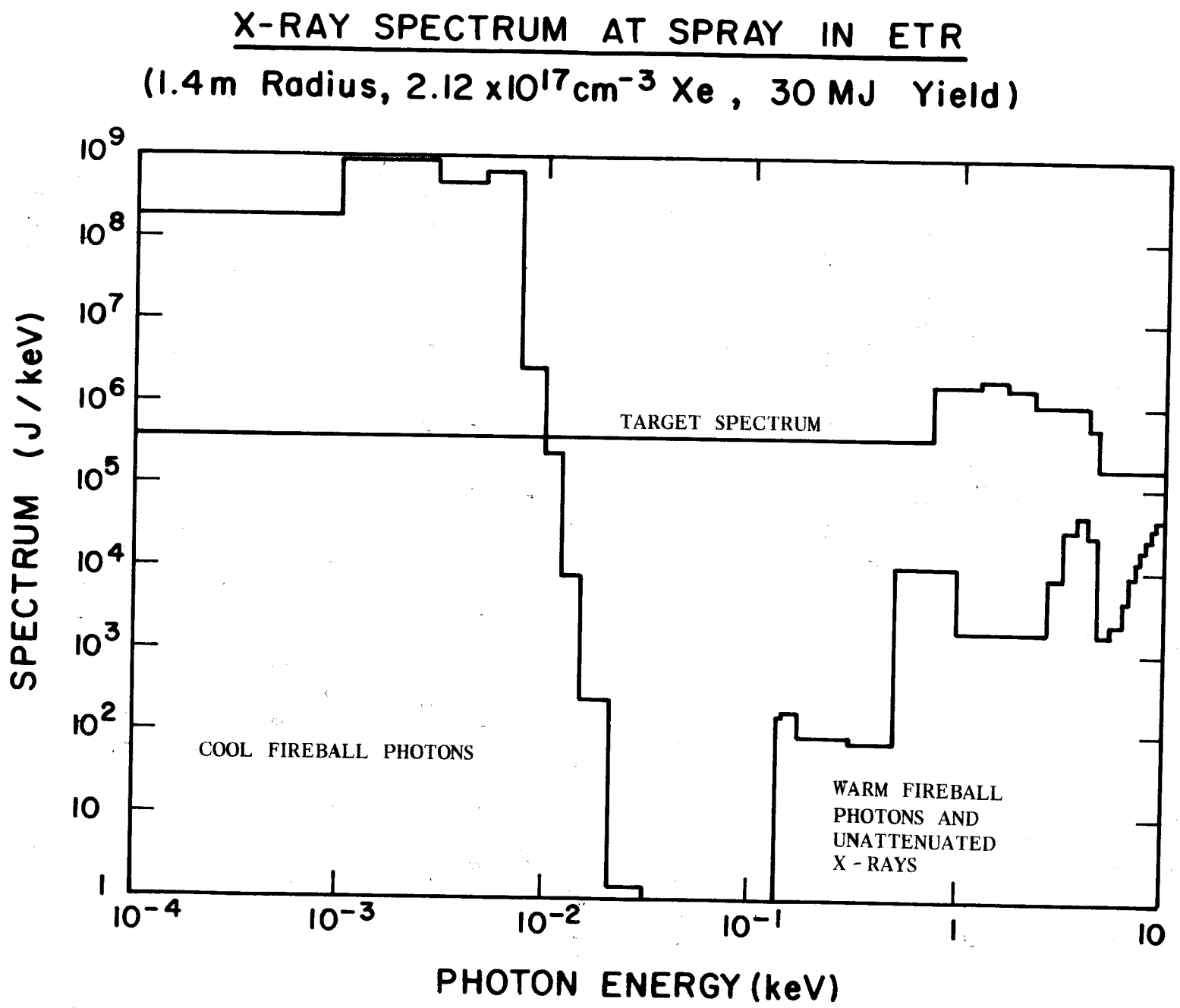

Figure 19. Radiant Heat and Unattenuated Target X-Ray Spectrum at Core/Mist Interface of ETR with No Lithium Vapor in the Core Integrated in Time. Target Spectrum is Also Shown for Comparison.

ETR and DEMO. The energy radiated to the interface by the time of arrival of the shock wave increases by a factor of 10 for the ETR and 150 for the DEMO when the lithium vapor is not present. This leads to increased vaporization of the mist which will establish a vapor concentration and a lower radiant energy density after a few shots. The steady state density of lithium has been estimated to be 3.12×10^{17} cm^{-3}. With this steady state density, the x-ray fluences and radiated energy density on the transport tubes as shown in Table 2 are not high enough to cause damage to a properly chosen material. The shock overpressures are not excessively large.

IV. Discussion

Several reactor relevant issues are introduced by the calculations outlined in Tables 1 and 2. These include: the possible acceleration of lithium drops up to speeds which may lead to wall erosion by the shock wave, the compression of the mist region and the resulting possible coalescence of drops, and the question of the fireball breakup and entrainment of the drops by the shock. The question of x-ray and fireball effects on the beam transport does not seem to be an issue which could put the design concept in jeopardy and was discussed earlier.

Fluid velocities in the mist can be as high as 4×10^4 cm/sec. It is an open question whether or not the drops are small enough for the shock to accelerate them significantly. In Lagrangian approaches to hydrodynamics such as this, it is very difficult to simulate a second fluid moving at a velocity different than the first so it is assumed that the drops, which could be a second fluid, are entrained in the gas and are, thus, moving at the same speed. The fluid used in these calculations is a mixture of mist, vapor and non-condensible gas and has a density, velocity and temperature which is an

average for the mixture as a whole. Thus, if the drops are not entrained, the fluid velocity of the gas would be higher because of both the dilution of the momentum of the dense slow drops and the lack of a shock reflecting density gradient in the fluid. If the shock does accelerate the drops, they may be deccelerated by the gas reflection off of the wall before the drops reach the wall. These are questions which cannot be addressed by the present analysis. In the worst case, drops with velocities of 4×10^4 cm/sec may strike the first wall and erode the wall.

In addition to entrainment, the drops may be broken up by the shock. Becoming smaller in size will increase the likelihood of entrainment. This connection with the discussion in the previous paragraph shows how uncertain these processes are; the breakup of drops is a difficult problem to analyze in itself but it makes the entrainment problem that much more difficult. In addition to entrainment, the breakup of drops should affect the rate of vaporization, but it has been shown that, within reasonably large bounds, the fireball propagation results are only mildly sensitive to the vaporization rate. The results presented here can provide input for calculations of the drop breakup.

Drops may also increase in size through the action of the fireball. Depending on the case considered, the mist region becomes compressed by as much as a factor of 20. The drops may end up 4 mm apart at the peak compression, compared to their original 1 cm spacing. However, since the average radius of the drop is 1 mm, there is not a great amount of coalescence.

The results presented here can be used to make certain statements concerning first wall design. The largest radiant energy on the walls of all of the cases is 7.1 J/cm^2 for the ETR in its cyclic steady state. This heat load

occurs in a pulse much less than a microsecond long but there is another longer term heat load resulting from condensation of lithium vapor onto the walls. In steady state, the total heat load must be 17 J/cm^2 for the ETR and 40 J/cm^2 for the DEMO. If the time over which this condensation heat flux is deposited is long compared to the temperature diffusion time in the wall, the radiant thermal load of 7.1 J/cm^2 is probably all that one must be concerned with. 7.1 J/cm^2 in a short pulse is near the limit for a bare metallic first wall and one may have to slightly increase the radius of the target explosion chamber. If, on the other hand, the lithium vapor condenses more quickly than the wall can conduct the heat away, a bare metallic wall is probably not a viable design. Analysis of the Sandia National Laboratory Target Development Facility (TDF), where the short term thermal heat load is approximately 40 J/cm^2, has been carried out at Wisconsin [8,9]. It was found that for the TDF, melting occurred in all bare first walls where several metals were tried. For a conservative design, it is now thought that one must use a sacraficial liner made of silicon carbide or graphite. If the condensation heat flux on the EAGLE first wall occurs over a short time, some design similar to the sacraficial liner approach could be proposed. The condensation time for the lithium vapor is currently unknown. The shock pressures are no larger than 4 atm and the TDF was designed for 17 atm so that this should not be a problem.

V. Conclusion

Modifications to the existing codes MIXERG and FIREMF have been made to account for the effects of vaporization on the gas dynamics of the EAGLE reactor. Results have been compiled for both the ETR and DEMO and the cyclic steady state and sensitivity of the results to the details of the vaporization have been investigated. Fluxes of target x-rays and thermal photons and me-

chanical loads have been calculated for the beam transport tubes and there does not appear to be a great problem in finding an acceptable design. Likewise, overpressures on the first walls are not prohibitively large. As long as the condensation time for the lithium vapor is long, a bare wall target chamber design may be possible. The results have been found to be only mildly sensitive to the details of vaporization.

The FIREMF code is not a two-phase flow code and no two-phase flow codes are known which also have multigroup radiative heat transfer. The radiative heat transfer is more important to this problem than the admitted two-phase nature of the mist and gas flow. It would be a very useful but difficult project to develop a two-phase flow multigroup radiative heat transfer hydrodynamics code with vaporization and condensation. The approach here has been the use of available codes and to use them with those modifications which can quickly be made and which account for physically dominant processes. It is strongly felt that vaporization of the lithium vapor is such a process and its effects have been included. Ultimately, the nature of gas dynamics in EAGLE type cavities will not be fully understood without experimental results.

Acknowledgment

This work was supported by Sandia National Laboratory under contract #71-5937 and by the Electric Power Research Institute through project #RP1527.

References

[1] R.R. Peterson and G.A. Moses, "MIXERG - An Equation of State and Opacity Computer Code," Computer Physics Communications 28 (1983) 405.

[2] G.A. Moses, T.J. McCarville and R.R. Peterson, "Documentation for MF-FIRE, A Multifrequency Radiative Transfer Version of FIRE," University of Wisconsin Fusion Engineering Program Report UWFDM-458 (March 1982).

[3] T.J. McCarville, R.R. Peterson and G.A. Moses, "Improvements in the FIRE Code for Simulating the Response of a Cavity Gas to Inertial Confinement Target Explosions," Computer Physics Communications 28 (1983) 367.

[4] R.R. Peterson, R.D. Watson, W.G. Wolfer and G.A. Moses, "TSTRESS - A Transient Stress Computer Code," University of Wisconsin Fusion Engineering Program Report UWFDM-382 (Dec. 1980).

[5] N.B. Vargaftik, Tables on the Thermophysical Properties of Liquids and Gases (John Wiley & Sons, Inc., New York).

[6] B. Badger et al., "HIBALL - A Conceptual Heavy Ion Beam Driven Fusion Reactor Study," Kernforschungszentrum Karlsruhe Report KfK 3202/ University of Wisconsin Fusion Engineering Program Report UWFDM-450 (Dec. 1981).

[7] R.O. Bangerter and D. Meeker, "Ion Beam Inertial Fusion Target Designs," Lawrence Livermore Laboratory Report UCRL-78474 (1976).

[8] R.R. Peterson et al., "First Wall Materials Selection in the Light Ion Beam Target Develoment Facility," Nuclear Technology/Fusion 4 (September 1983) 872.

[9] E.G. Lovell and R.L. Engelstad, "Dynamic Stress Analysis of Light Ion Fusion," Nuclear Technology/Fusion 4 (September 1983) 878.